Jones et al., http://www.jcb.org/cgi/content/full/jcb.201408025/DC1



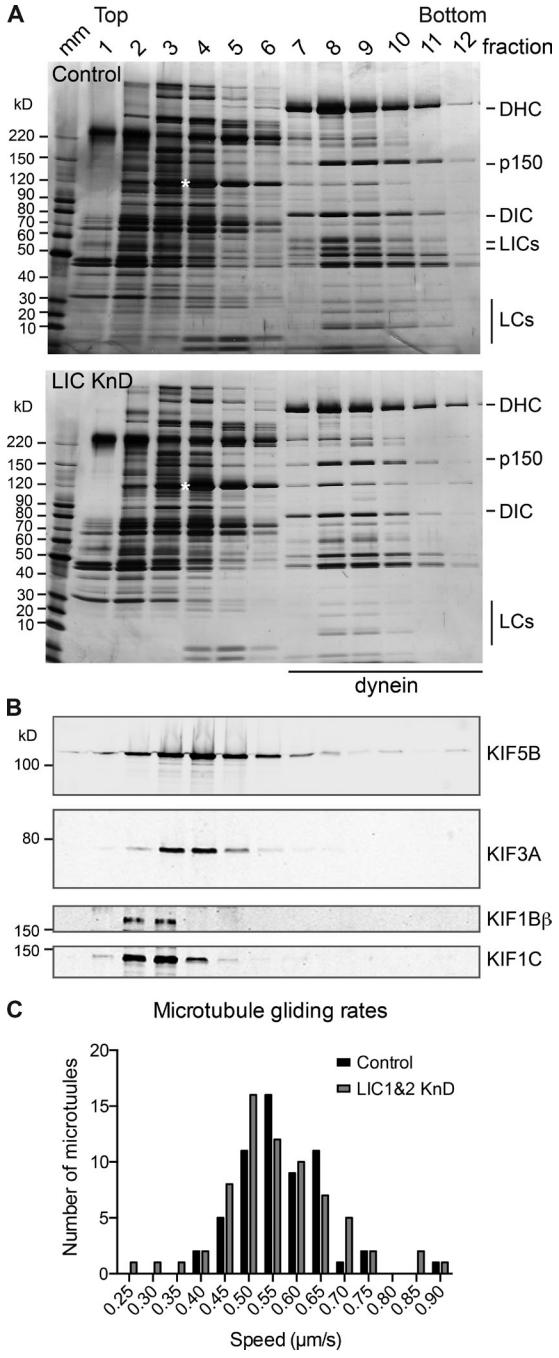


Figure S1. **Biochemical analysis of microtubule motors.** (A) Microtubule motors isolated from control and LIC-depleted HeLaM cells were separated on sucrose density gradients and analyzed by SDS-PAGE and silver staining. Asterisks indicate kinesin-1 heavy chain; mm indicates the molecular mass marker lane, and numbers correspond to gradient fractions (1 = top; 12 = bottom). A side-by-side comparison of the peak dynein fraction from control and LIC-depleted cells is shown in Fig. 1. The dynein with and without LICs migrates at the same position on the gradient and contains similar proportions of IC and light chains (LC), indicating that its structure is unaffected by LIC loss. Dynactin is also present in similar amounts and migrates at the same density in both samples. The remaining band at ~60 kD in the LIC-depleted dynein fractions is likely to be the dynactin p62 subunit. The molecular mass maker sizes are shown in kilodaltons. (B) Immunoblotting of a control microtubule motor preparation using the indicated antibodies to kinesin family members shows that sucrose density gradient centrifugation effectively separates dynein from kinesins. (C) Histogram of microtubule gliding rates in vitro generated by purified dynein with and without LICs (58 and 67 microtubules, respectively, from three independent experiments).

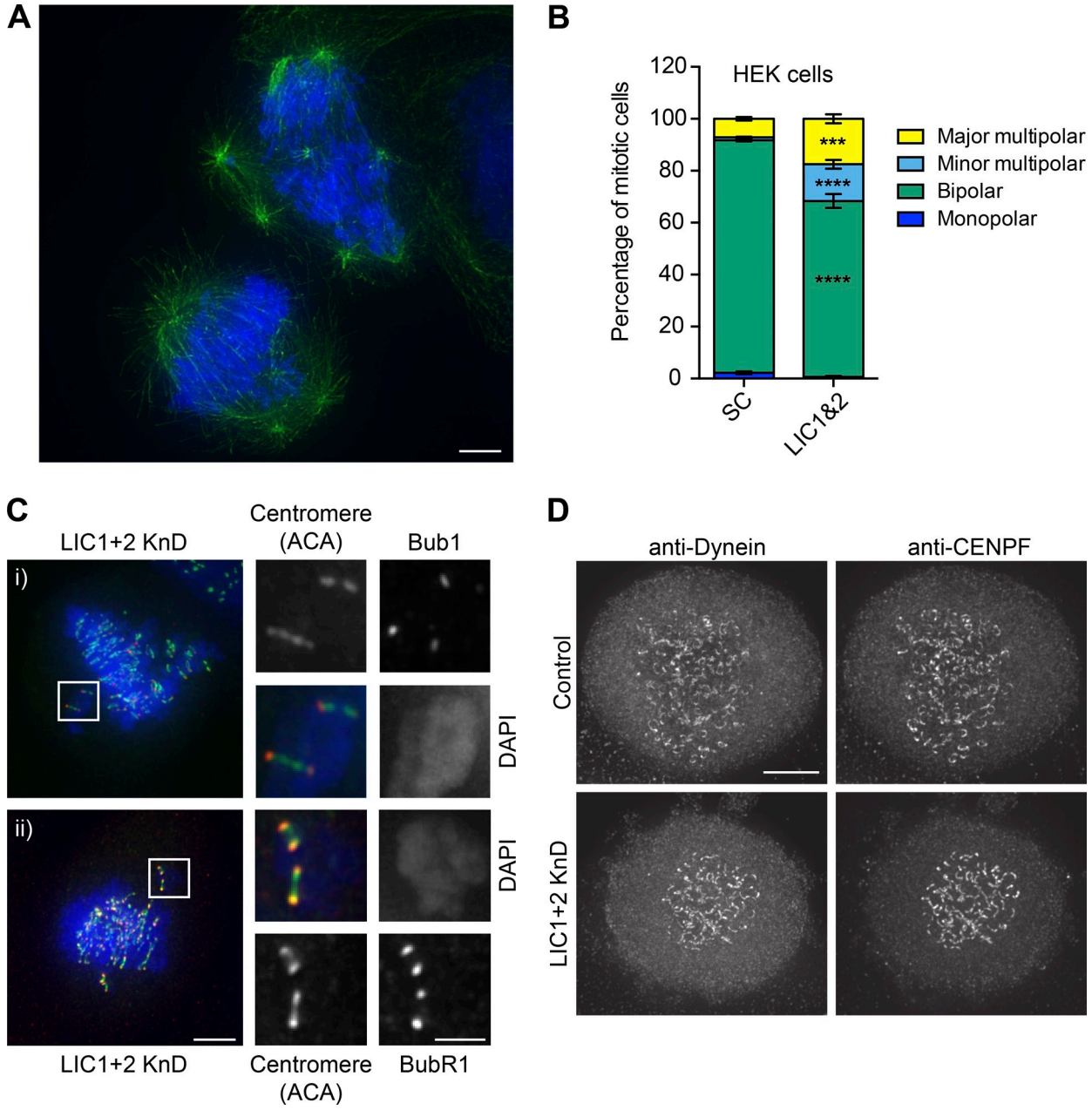


Figure S2. **Effect of LIC loss on spindle morphology and kinetochores.** (A–D) HeLaM (A, C, and D) or HEK (B) cells were transfected with scrambled siRNAs or a combination of LIC1 and LIC2 siRNAs and then fixed 72 h later, labeled, and imaged. (A) A DeltaVision deconvolved z series projection showing a major multipolar (top cell) and minor multipolar (bottom cell) phenotype in HeLaMs labeled with anti–α-tubulin and DAPI. (B) The phenotype of mitotic HEK cells was scored (>650 cells in total from three independent experiments; means ± SEM). P-values from two-way ANOVA with Sidak's multiple comparison test for control versus LIC depletion: ***, $P < 0.001$; ****, $P < 0.0001$. SC, scrambled. (C) LIC-depleted HeLaM cells were labeled with antibodies to the centromere (anticentromere antibodies [ACA]), Bub1, or BubR1 to visualize the kinetochores. Deconvolved z-series projections are shown, with enlargements of the boxed regions. (D) HeLaM cells depleted of both LICs, or untreated cells, were treated with 10 µM nocodazole for 60 min to depolymerize microtubules, fixed, and labeled with antibodies to IC and CENP-F, which localizes to kinetochores. Images are projections of a z series of deconvolved images. Bars: (A and C, main images) 5 µm; (C, enlarged images) 2 µm; (D) 10 µm.

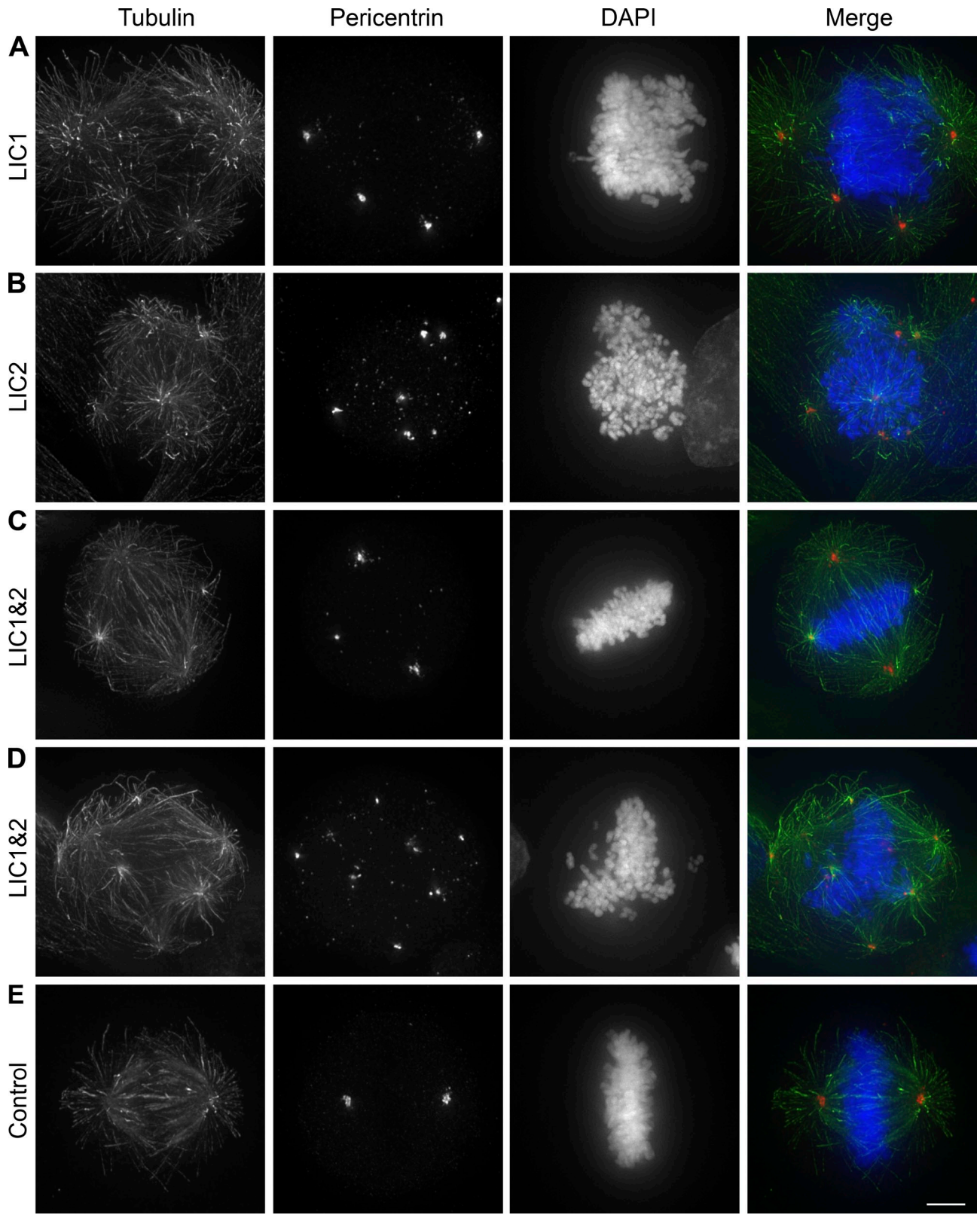


Figure S3. **PC localizes to the centrosome in LIC1, LIC2, and LIC1 and 2 siRNA-treated HeLaM cells.** (A–E) HeLaM cells depleted of LIC1 (A), LIC2 (B), both LIC 1 and 2 (C, minor multipolar spindle; D, major multipolar spindle), or untreated cells (E) were labeled with DAPI (blue), anti–α-tubulin (green), and anti-PC (red) and imaged on a DeltaVision microscope. Maximum projections of deconvolved z-series stacks are shown. Bar, 5 µm.

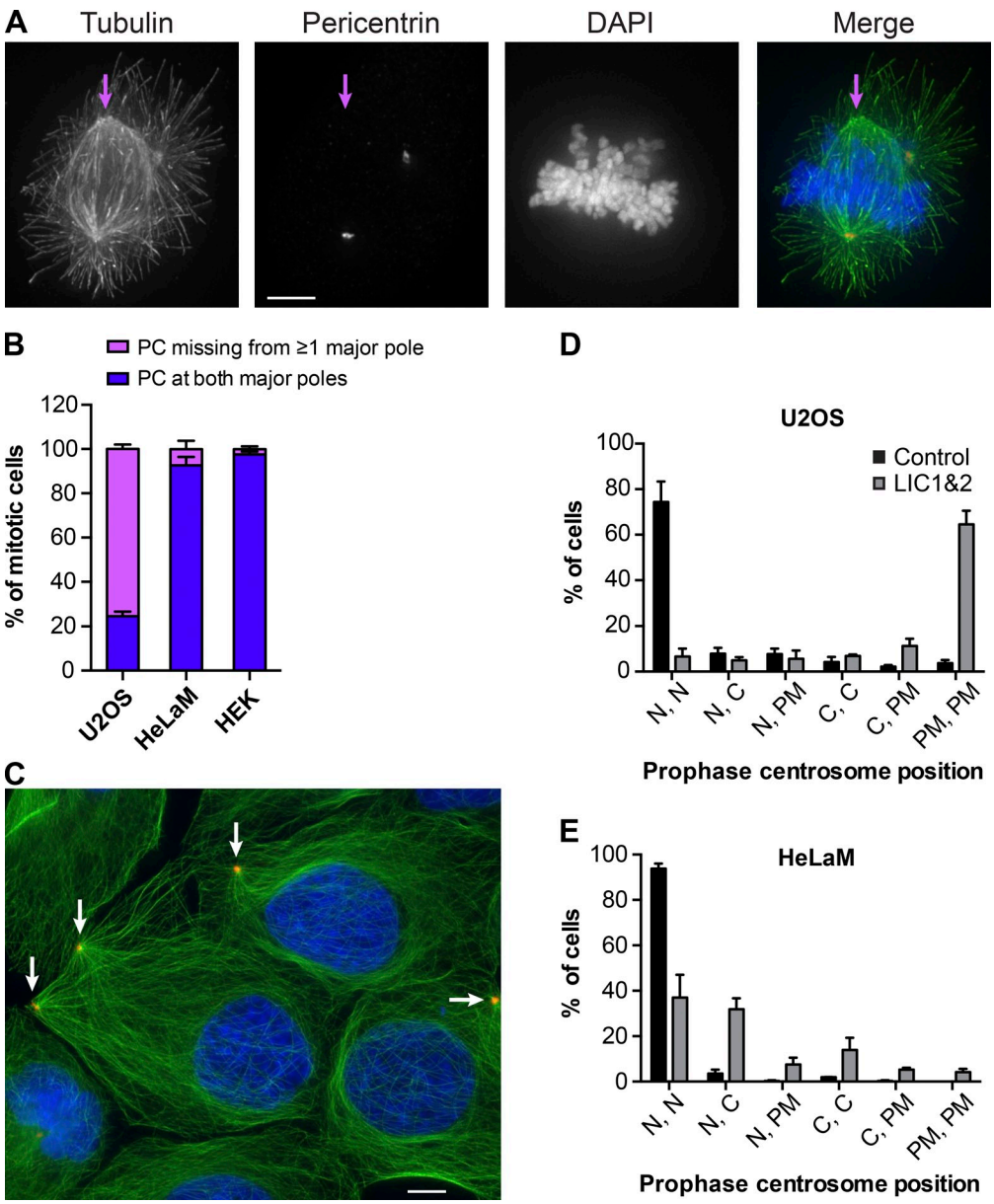


Figure S4. **Effect of LIC depletion on spindle assembly, pole composition, and prophase centrosome position in U2OS and HEK cells.** (A) U2OS cells depleted of both LICs were labeled with anti–α-tubulin (green), anti-PC (red), and DAPI (blue) and imaged on a DeltaVision microscope. A maximum projection of a deconvolved z-series stack is shown. (B) Cell line–specific differences in PC composition of spindle poles in cells with minor multipolar spindles. The two major poles of each minor multipolar spindle were scored for whether they possessed PC. As an example, the cell in A has one major pole that lacks PC (magenta arrows). A total of 433 (HeLaM), 294 (U2OS), and 92 HEK cells were scored from three to four independent experiments (means ± SEM). (C) LIC-depleted interphase U2OS cells with mispositioned centrosomes (arrows). Cells were labeled an imaged as in A except that a projection was made using the ImageJ extended focus plugin. (D and E) The position of each centrosome in prophase U2OS (D) and HeLaM (E) cells was scored: N, adjacent to the nucleus; C, cytoplasmic (see middle cell, image in C); PM, next to the plasma membrane (left cell, image in C). A total of ≥266 HeLaM cells from four independent experiments and ≥240 U2OS cells from three independent experiments were scored (means ± SEM). Bars, 5 µm.

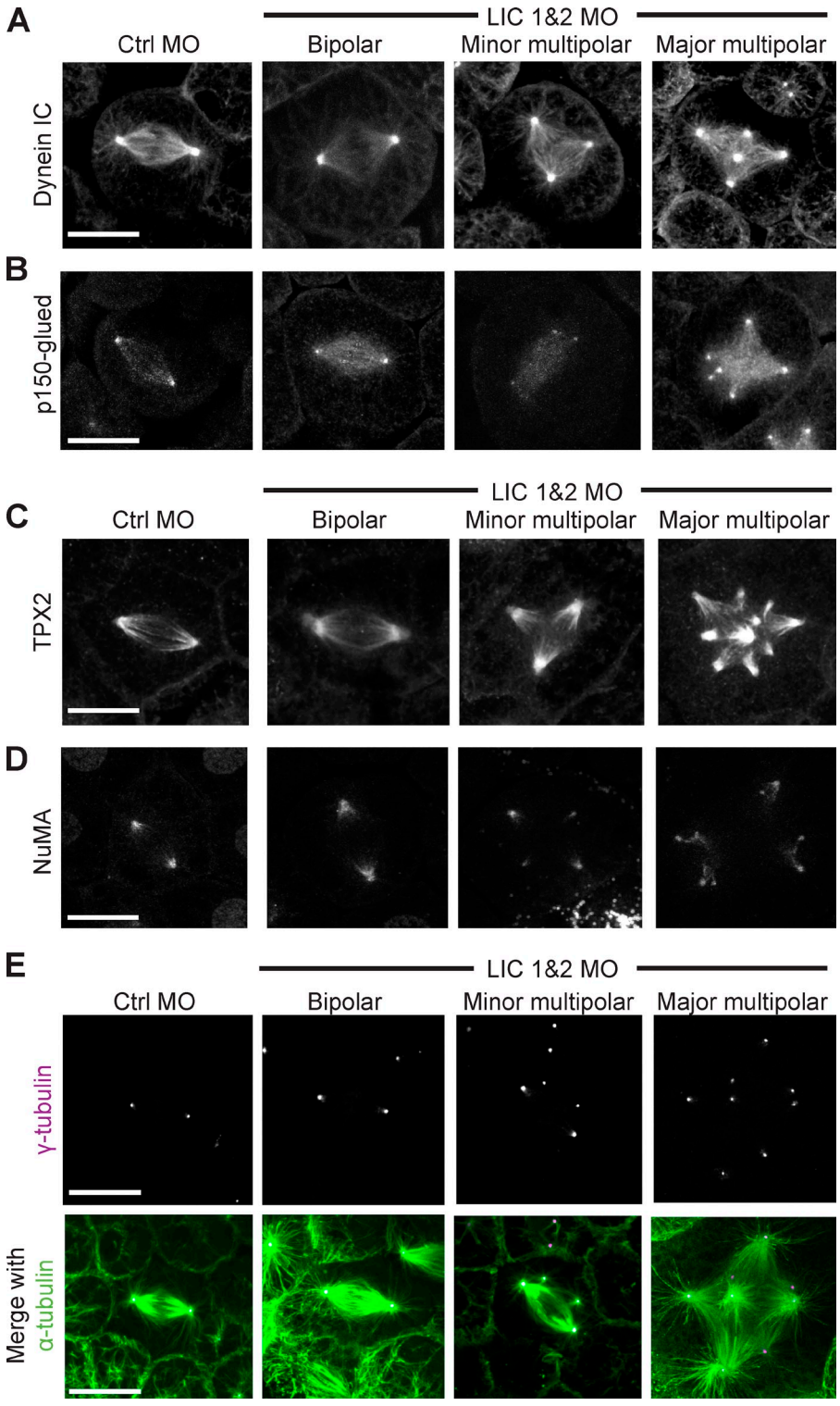


Figure S5. **Dynein, dynactin, and spindle assembly factors localize normally to LIC1- and 2-depleted spindles.** (A–E) Immunofluorescence was used to determine the localization of dynein (A, anti–*Xenopus* IC), dynactin (B, p150-glued), TPX2 (C), NuMA (D), and γ-tubulin (E) in control (Ctrl MO) and LIC1 and 2 (LIC1&2 MO) MO-injected *Xenopus* embryos. All were found to localize normally in LIC1 and 2 morphant spindles irrespective of whether they were bipolar (two poles) or multipolar (three to four or greater than five poles) spindles. Bars, 20 µm.

Table S1. **Statistical analysis of the effects of inhibition of Eg5 on spindle morphology, in combination with LIC depletion**

| Eg5 inhibition | | *Xenopus* Eg5 inhibition p-value | | | HeLaM Eg5 inhibition p-value | | |
|---|---|---|---|---|---|---|---|
| **Condition** | **Spindle morphology** | **C + DMSO** | **C + STLC** | **LIC + DMSO** | **SC + DMSO** | **SC + STLC** | **LIC + DMSO** |
| Control KnD + STLC | Monopolar | ≤0.0001 | – | – | ≤0.0001 | – | – |
| | Bipolar | ≤0.0001 | – | – | ≤0.0001 | – | – |
| | Minor multiple | NS | – | – | NS | – | – |
| | Major multiple | NS | – | – | NS | – | – |
| LIC KnD + DMSO | Monopolar | NS | ≤0.0001 | – | NS | ≤0.0001 | – |
| | Bipolar | ≤0.0001 | ≤0.0001 | – | ≤0.0001 | ≤0.0001 | – |
| | Minor multiple | ≤0.0001 | ≤0.0001 | – | ≤0.0001 | ≤0.0001 | – |
| | Major multiple | ≤0.0001 | ≤0.0001 | – | NS | ≤0.01 | – |
| LIC KnD + STLC | Monopolar | ≤0.01 | ≤0.0001 | ≤0.01 | ≤0.0001 | ≤0.0001 | ≤0.0001 |
| | Bipolar | ≤0.0001 | ≤0.0001 | ≤0.0001 | ≤0.0001 | ≤0.0001 | ≤0.0001 |
| | Minor multiple | ≤0.05 | ≤0.05 | ≤0.0001 | NS | NS | ≤0.0001 |
| | Major multiple | ≤0.0001 | ≤0.0001 | NS | NS | NS | ≤0.01 |

The data presented graphically in Fig. 9 (A, B, D and E) were analyzed by two-way ANOVA with Tukey's test. For Eg5 inhibition in *Xenopus* embryos, 39–41 embryos were analyzed for each condition, assessing a total of between 375 and 1,175 spindles for spindle morphology, $n = 6$ independent experiments. For HeLaM Eg5 inhibition, a total of 427–485 cells were scored from four independent experiments (>100 per condition). Minus signs indicate comparisons that are made elsewhere in the table. C, control; SC, scrambled.

Table S2. **Statistical analysis of the effects of Nuf2 depletion and inhibition CENP-E on spindle morphology, in combination with LIC depletion**

| Nuf2 and CENP-E inhibition | | HeLaM Nuf2 depletion p-value | | | HeLaM CENP-E inhibition p-value | | |
|---|---|---|---|---|---|---|---|
| **Condition** | **Spindle morphology** | **SC + SC KnD** | **SC + Nuf2 KnD** | **LIC + Nuf2 KnD** | **SC + DMSO** | **SC + CI** | **LIC + DMSO** |
| SC KnD + treatment | Monopolar | NS | – | – | NS | – | – |
| | Bipolar | ≤0.0001 | – | – | ≤0.0001 | – | – |
| | Minor multiple | ≤0.0001 | – | – | ≤0.0001 | – | – |
| | Major multiple | ≤0.05 | – | – | NS | – | – |
| LIC KnD + control treatment | Monopolar | NS | NS | – | NS | NS | – |
| | Bipolar | ≤0.0001 | ≤0.0001 | – | ≤0.0001 | ≤0.0001 | – |
| | Minor multiple | ≤0.0001 | ≤0.0001 | – | ≤0.0001 | NS | – |
| | Major multiple | ≤0.01 | NS | – | ≤0.0001 | ≤0.0001 | – |
| LIC KnD + treatment | Monopolar | NS | NS | NS | NS | NS | NS |
| | Bipolar | ≤0.0001 | ≤0.0001 | ≤0.0001 | ≤0.0001 | ≤0.0001 | ≤0.01 |
| | Minor multiple | ≤0.0001 | ≤0.0001 | NS | ≤0.0001 | ≤0.0001 | ≤0.001 |
| | Major multiple | ≤0.0001 | ≤0.0001 | ≤0.0001 | ≤0.0001 | ≤0.0001 | NS |

The data presented graphically in Fig. 9 (A, B, D and E) were analyzed by two-way ANOVA with Tukey's test. For HeLaM Nuf2 depletion experiments, a total of 854–872 cells were scored from four independent experiments (>200 per condition). For HeLaM CENP-E inhibition, a total of 412–438 cells were scored from four independent experiments (>100 per condition). Minus signs indicate comparisons that are made elsewhere in the table. SC, scrambled; CI, CENP-E inhibitor.

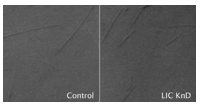


Video 1. **Loss of LIC does not affect dynein motor function in vitro.** Microtubule gliding driven by dynein purified from control (left) or LIC KnD HeLaM cells (right). Imaging was performed by video-enhanced differential interference contrast microscopy (BX60; Olympus) at RT at 25 frames per second using a video camera (Newvicon) and image processor (Argus-10) and is played back at 4× real time. Each panel is 13.5-µm across. Videos are viewed best using QuickTime 7.

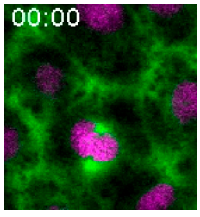


Video 2. **Mitotic spindle in a control morphant.** Live confocal imaging of a mitotic spindle in a *Xenopus* gastrula stage embryo injected with a standard control MO. GFP–α-tubulin (green) was used to label microtubules and chromosomes were visualized using mCherry-Histone2B (magenta). Single focal plane images were collected every 6 s using a confocal microscope (FluoView FV1000; Olympus) with a 60×, 1.35 NA U Plan S Apochromat objective. Time-lapse videos were constructed in ImageJ and play back at a speed of 7 frames per second. The time stamp indicates time in minutes and seconds.

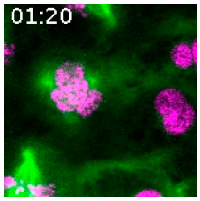


Video 3. **Multipolar spindle assembly in a LIC1 and 2 morphant.** Live confocal imaging of a mitotic spindle in a *Xenopus* gastrula stage embryo injected with both LIC1 and LIC2 MOs. GFP–α-tubulin (green) was used to label microtubules, and chromosomes were visualized using mCherry-Histone2B (magenta). The spindle assembles with three poles. Single focal plane images were collected every 10 s using a confocal microscope (FluoView FV1000; Olympus) with a 60×, 1.35 NA U Plan S Apochromat objective. Time-lapse videos were constructed in ImageJ and play back at a speed of 12 frames per second. The time stamp indicates time in minutes and seconds.

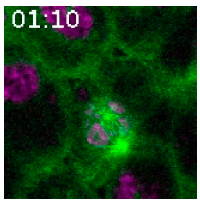


Video 4. **Pole fragmentation of a bipolar spindle in a LIC1 and 2 morphant.** Live confocal imaging of a mitotic spindle in a *Xenopus* gastrula stage embryo injected with both LIC1 and LIC2 MOs. GFP–α-tubulin (green) was used to label microtubules and chromosomes were visualized using mCherry-H2B (magenta). A bipolar spindle assembles but then undergoes spindle pole fragmentation: the first pole begins to fragment at ~24 min and 20 s, and the second fragments at 36 min. Single focal plane images were collected every 10 s using a confocal microscope (FluoView FV1000; Olympus) with a 60×/1.35 NA U Plan S Apochromat objective. Time-lapse videos were constructed in ImageJ and play back at a speed of 12 frames per second. The time stamp indicates time in minutes and seconds.

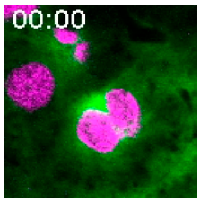


Video 5. **A multipolar spindle assembles in a LIC1 and 2 morphant and then undergoes pole fragmentation.** Live confocal imaging of a mitotic spindle in a *Xenopus* gastrula stage embryo injected with both LIC1 and LIC2 MOs. GFP–α-tubulin (green) was used to label microtubules and chromosomes were visualized using mCherry-H2B (magenta). The spindle assembles with three poles, but at ~20 min and 20 s, one of these poles fragments. Single focal plane images were collected every 10 s using a confocal microscope (FluoView FV1000; Olympus) with a 60×, 1.35 NA U Plan S Apochromat objective. Time-lapse videos were constructed in ImageJ and playback at a speed of 12 frames per second. The time stamp indicates time in minutes and seconds. To recenter the spindle in the field of view, the video position was adjusted at 17 min and 30 s.

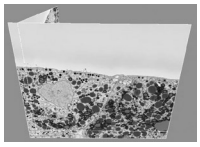

Video 6. **3View EM of a control spindle.** A 3D reconstruction of a mitotic spindle in the epithelium of a control *Xenopus* morphant gastrula stage embryo. Images were collected using a microtome (3View; Gatan) within a scanning electron microscope (Quanta 250 FEG; FEI) with sections taken 100 nm apart. The imaging conditions were indicated quadrant magnification of 1,600×, accelerating voltage of 3.8 kV, pressure at 0.33 Torr, image at 4,000 × 5,000 pixels, and dwell time of 10 µs. Images were reconstructed using Imaris image analysis software (Bitplane). Chromosomes (blue) and centrioles (red) were reconstructed in Imaris using the Surfaces tool. Note that each pole of the bipolar spindle contains a pair of centrioles.

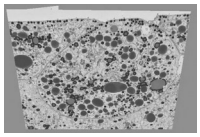

Video 7. **3View EM of a LIC KD multipolar spindle.** A 3D reconstruction of a mitotic spindle in the epithelium of a *Xenopus* morphant injected with both LIC1 and 2 MOs. Images were collected using a microtome (3View; Gatan) within a scanning electron microscope (Quanta 250 FEG; FEI) with sections taken 100 nm apart. The imaging conditions were as follows: indicated quadrant magnification of 1,600×, accelerating voltage of 3.8 kV, pressure at 0.33 Torr, images of 4,000 × 5,000 pixels, and dwell time of 10 µs. Images were reconstructed using Imaris image analysis software (Bitplane). Chromosomes (blue) and centrioles (red) were reconstructed in Imaris using the Surfaces tool. Note that all poles of the multipolar spindle contain only a single centriole.

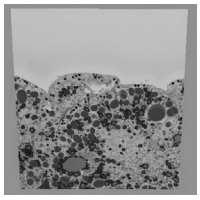

Video 8. **3View EM of a LIC KD bipolar spindle.** A 3D reconstruction of a mitotic spindle in the epithelium of a *Xenopus* morphant injected with both LIC1 and 2 MOs. Images were collected using a microtome (3View; Gatan) within a scanning electron microscope (Quanta 250 FEG; FEI) with sections taken 100 nm apart. The imaging conditions were as follows: indicated quadrant magnification of 1,600×, accelerating voltage of 3.8 kV, pressure at 0.33 Torr, images of 4,000 × 5,000 pixels, and dwell time of 10 µs. Images were reconstructed using Imaris image analysis software (Bitplane). Chromosomes (blue) and centrioles (red) were reconstructed in Imaris using the Surfaces tool. Note that although each pole contains two centrioles, these centrioles are further apart than is seen in the control bipolar spindle (Video 6).